THE PRINCETON MAGNETOROTATIONAL INSTABILITY EXPERIMENT

E. Schartman[1], H. Ji[1], M. Burin[1], S. Raftopoulos[1], R. Cutler[1],
P. Heitzenroeder[1], W. Liu[1], J. Goodman[2], J. Stone[2], A. Kageyama[3]

[1] *Princeton Plasma Physics Laboratory, Princeton University, New Jersey, USA*
[2] *Department of Astrophysics, Princeton University, Princeton, New Jersey, USA*
[3] *Earth Simulator Center, Yokohama, Japan*

Introduction. For nearly 30 years it was known in astrophysics that the accretion of orbiting matter onto a compact central object drives the luminosity of systems such as Active Galactic Nuclei, neutron stars, black holes and white dwarfs, and that it is also fundamental to star formation. Finding plausible mechanisms for the underlying angular momentum transport initially proved quite difficult. Ordinary viscosity is orders of magnitude too weak, and these accretion disks being centrifugally stable, are immune to the Rayleigh–Taylor instability. For these reasons, it was long suspected that enhanced viscosity due to MHD turbulence is responsible. In 1991 Balbus & Hawley[1] rediscovered [2, 3] that for angular velocity decreasing with radius, the stretching of a weak magnetic field can transfer angular momentum between fluid elements at different radii leading to instability. Much theoretical and numerical work[4] on this MagnetoRotational Instability (MRI) has shown that it is a powerful mechanism for the transport of angular momentum. Despite its fundamental, and growing role in astrophysics, the MRI has not been conclusively detected in the laboratory. The goals of this experiment are to achieve a clear demonstration of the MRI in a liquid gallium Taylor–Couette (TC) flow, to study its angular momentum transport properties and saturation. These results will then provide a benchmark for numerical codes used to simulate astrophysical flows.

1. The magnetorotational instability. An extensive literature exists on the MRI relevant to both accretion disks[5], and liquid metal TC flow[6]. In cylindrical geometry, consider a perfectly conducting, inviscid fluid whose rotation axis is parallel to an external magnetic field, $\mathbf{B}_z$. Two fluid elements sharing a field line can be thought of as masses connected by a spring, in orbit about a central mass. Maxwell stress in the field acts as the spring constant, see Fig. 1a. For gravity, angular velocity is a decreasing function of radius, $\Omega \sim r^{-3/2}$. So, if mass m_i is perturbed radially inward to larger rotation rates, it will feel a deceleration due to the stretching of the spring. This will reduce its kinetic energy, causing it to fall further inward. Conversely, on the other end of the spring mass m_o will be pulled forward, increasing its kinetic energy and causing it to move to larger radii and slower angular velocity. If the spring is sufficiently weak that its period is much longer than that of the orbit, this process will run away. First order consideration[5] with density ρ, angular velocity $\Omega(r)$, and time and spatial variation $\sim exp(-i\omega t + i\mathbf{k} \cdot \mathbf{r})$ leads to the dispersion relation:

$$\omega^4 - \omega^2[\kappa^2 + 2(\mathbf{k} \cdot \mathbf{u}_A)^2] + (\mathbf{k} \cdot \mathbf{u}_A)^2 \left\{ (\mathbf{k} \cdot \mathbf{u}_A)^2 + \frac{\partial \Omega^2}{\partial \ln r} \right\} = 0.$$

Here $\kappa^2 = r^{-3}\partial r^4 \Omega^2 / \partial r$ is the epicyclic frequency, and $u_A^2 = B^2/4\pi\rho$ is the Alfvén speed. Instability is determined by the term in braces: growing modes
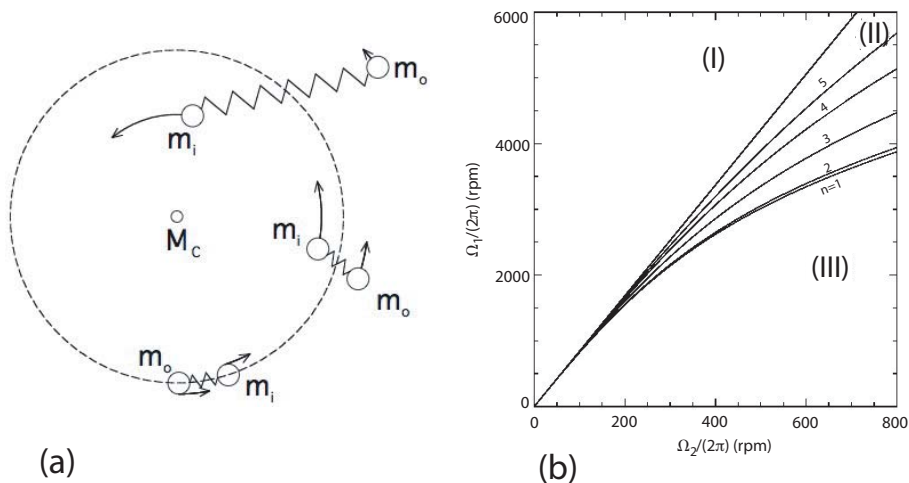
Fig. 1. (*a*) The linear MRI is dynamically equivalent to orbiting masses connected by a weak spring. Arrows represent angular velocity. (*b*) Stability diagram of a Taylor–Couette flow of liquid Gallium with experimentally feasible geometry should be unstable to several modes.

occur for $-\partial\Omega^2/\partial \ln r > (\mathbf{k} \cdot \mathbf{u}_A)^2$, with a minimum growth time given by $\tau_{MRI} \sim (\partial\Omega/\partial \ln r)^{-1}$. For fixed wavenumber, the MRI is present for some small B so long as angular velocity decreases with radius. If the smallest k_z is twice the height, h, of the fluid volume, then the MRI is quenched when B exceeds $4\pi\rho h\partial\Omega^2/\partial \ln r$. That the instability does not vanish as $B \to 0$, but does at finite B is the hallmark of the MRI.

The dispersion relation was arrived at by consideration of a gravitationally bound fluid. But the MRI is not restricted to gravity. The identical relation can also be arrived at for TC flow, $\Omega \sim r^{-2}$, where the profile is established by viscous radial angular momentum transport for a fluid confined between concentric, co-rotating cylinders of infinite height.

Viscosity, ν, and resistivity, η, both limit the growth of the MRI. In particular, resistivity eliminates growth as $B \to 0$, as too weak a B field will diffuse back to its equilibrium configuration before fluid elements are able to move significantly. Although accreting astrophysical plasmas are nearly perfectly conducting, resistive MRI is likely to be relevant to protostellar disks, and Cepheid variables in the quiescent state. A stability analysis [7] of the MRI for an experimentally realizable TC flow was performed. Liquid Gallium is the choice of working fluid with $\rho = 6.3 \times 10^3 \, \text{kg/m}^3$, $\nu = 3 \times 10^{-7} \, \text{m}^2/\text{s}$ and $\eta = 0.2 \, \text{m}^2/\text{s}$. Figure 1$b$ shows three regimes of stability for magnetized TC flow as a function of inner and outer cylinder speed. In region (I) the Rayleigh–Taylor stability criterion is not met, and the flow is hydrodynamically unstable, though the application of a magnetic field can restore stability. An experiment [8] has claimed a detection of MRI-like modes in Region (I). Region (III) is always stable. Region (II) is hydrodynamically stable, but several axial modes of the MRI can be excited in the presence of a vertical magnetic field. This regime is most relevant to accretion disks and prior to this experiment has not been studied.

2. Experimental apparatus and operation. The design of our experiment aims to produce the MRI in conditions as simple and repeatable as possible: a liquid Gallium Couette flow in the presence of an axial solenoidal magnetic field. The flow is established between two stainless steel, concentric, co-rotating cylin-

ders of radii $r_1 = 0.07$ m and $r_2 = 0.21$ m. To balance the likelihood of generating the MRI with minimizing the amount of Gallium (and hence expense) required, the cylinder height, $h = 0.28$ m was chosen to be twice the gap width $r_2 - r_1$. After working with a water-filled prototype we determined [9] that boundary effects would produce an unfavorable velocity profile. The solution we have implemented is to divide the end caps into two differentially rotating rings, see Fig. 2. The cylinders have maximum speeds of $\Omega_1/2\pi = 4000$ rpm and $\Omega_2/2\pi = 600$ rpm, while the inner and outer end rings rotate at up to 2000 rpm, and 1000 rpm, respectively. The four rotating elements are driven by separate DC motors, all controlled by a PC running LabView. The magnetic field is generated by six field coils with inner diameters ~ 0.6 m, with maximum field strength ~ 0.8 T.

2.1. Torque.   Measurement of the effective fluid viscosity coupling the inner and outer cylinders is the most direct diagnostic of enhanced angular momentum transport. Two methods are employed to measure this coupling on timescales both long and short compared to τ_{MRI}. A load cell mounted on each motor measures the torque being input to the apparatus, and is limited by the servo loop time constant. To capture changes in coupling within $\tau_{MRI} \sim 50$ ms, a digitized optical encoder signal is used acquire component speed variations within 10 ms.

2.2. Fluid profile.   Before proceeding to Gallium operation, the hydrodynamic effect of the split end-ring design was characterized using Particle Tracking Velocimetry. The results of these experiments [10] show that Ekman circulation has been reduced such that deviations from the ideal Couette profile are dominated by the stewartson layer formed at the end ring gap. During Gallium operation, the flow will be characterized using a combination of Ultrasonic Speckle Velocimetry (USV), acoustics and hot wire or Hall probes.
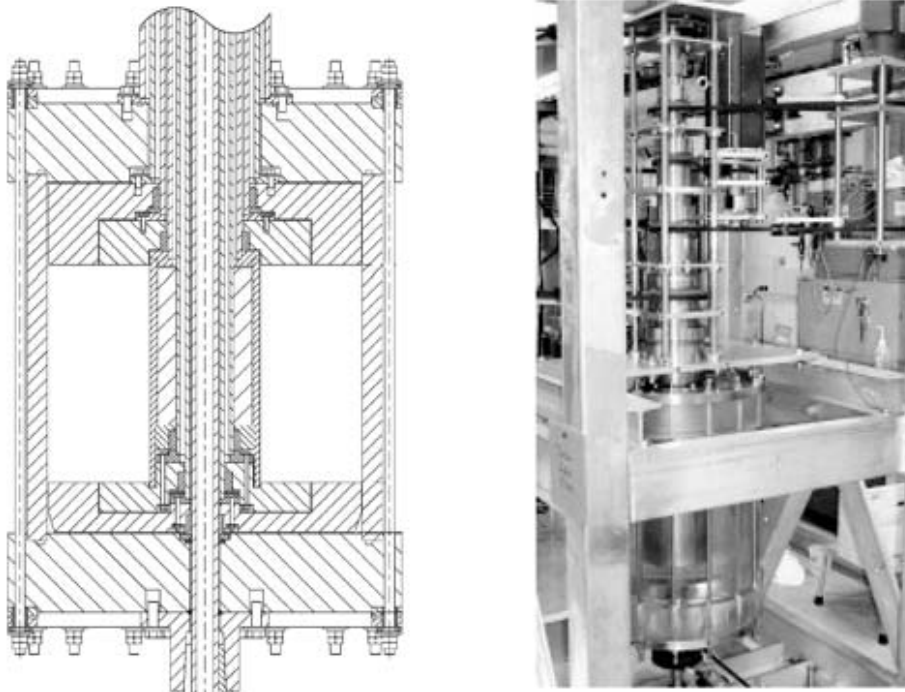

Fig. 2. The Princeton MRI experiment: cross sectional view of the experimental volume, left. Apparatus as it appeared during water operation, right.

2.3. Magnetic field. Due to the action of the MRI, the initially vertical magnetic field will be sheared radially and azimuthally. The radial component will propagate outside the insulating boundaries of the fluid. An array of magnetic probes placed between the magnet coils and the outer cylinder will detect this radial field. Azimuthal perturbations may be measured using these sensors mounted in a low-drag fin inserted into the fluid. The arrays will consist of Hall sensors (DC to a few kHz) and inductive probes (up to MHz), and will be sensitive to perturbations at the 0.1 G level.

2.4. Experiment operation. Our search for the MRI is comprised of the following three phases.

1. **Water.** Effectiveness of split-end ring design has been verified [10]. Characterization of high-Re profile will next occur. These data will provide a benchmark for a 3D simulation at Re $\sim$ 6000.

2. **Initial Gallium MHD experiments.** Study magnetized TC flow in MRI-stable regime to characterize interaction of residual ekman circulation, stewartson layers with magnetic field.

3. **Gallium MRI operation.** Generate an MRI-unstable velocity profile, slowly ramp up the B field until instability occurs. Observe MRI in both linear growth and saturated regimes, repeating measurements for a variety of B-field magnitudes and rotation profiles.

3. Summary. The Princeton MRI experiment is uniquely positioned to provide a concrete detection of the MRI, and study some of its properties in an astrophysically relevant context. This study will also provide a valuable benchmark for the codes that are used to simulate rotating astrophysical flows.

REFERENCES

1. S.A. BALBUS, J.F. HAWLEY. *Astrophys. J.*, vol. 376 (1991), pp. 214–222.

2. S. CHANDRASEKHAR. *Hydrodynamic and Hydromagnetic Stability* (Oxford Univ. Press, London, 1961).

3. E.P. VELIKHOV. *Sov. Phys. JETP*, vol. 36 (1959), pp. 995–998.

4. S.A. BALBUS AND J.F. HAWLEY. *Rev. Mod. Phys.*, vol. 70 (1998), pp. 1–53.

5. S.A. BALBUS. *Annu. Rev. Astron. Astrophys.*, vol. 41 (2003), pp. 555–597.

6. J. GOODMAN, H. JI. *J. Fluid Mech.*, vol. 462 (2002), pp. 365–382.

7. H. JI, J. GOODMAN, A. KAGEYAMA, *MNRASV*, vol. 325 (2001), pp. L1–L5

8. D.R. SISAN, N. MUJICA, W.A. TILLOTSON, Y. HUANG, W. DORLAND, A.B. HASSAM, T.M. ANTONSEN, D.R. LATHROP. *Phys. Rev Lett.V*, vol. 93, pp. 114502-1–114502-4

9. A. KAGEYAMA, H. JI, J. GOODMAN, F. CHEN, E. SHOSHAN. *J. Phys. Soc. Jap*, vol. 73 (2004), pp. 2424–2437.

10. M. BURIN, E. SCHARTMAN, H. JI, L. MORRIS, S. RAFTOPOULOS, R. CUTLER . In preparation.